

# Experimental demonstration of a tomographic 5D phase-space reconstruction

S. Jaster-Merz,<sup>1,\*</sup> R. W. Assmann,<sup>1,†</sup> J. Beinortaitė,<sup>1</sup> J. Björklund Svensson,<sup>1,‡</sup> R. Brinkmann,<sup>1</sup> F. Burkart,<sup>1</sup> P. Craievich,<sup>2</sup> H. Dinter,<sup>1</sup> P. González Caminal,<sup>1,§</sup> W. Hillert,<sup>3</sup> A. L. Kanekar,<sup>1</sup> M. Kellermeier,<sup>1</sup> W. Kuropka,<sup>1</sup> F. Mayet,<sup>1</sup> J. Osterhoff,<sup>1,¶</sup> B. Stacey,<sup>1</sup> M. Stanitzki,<sup>1</sup> T. Vinatier,<sup>1</sup> S. Wesch,<sup>1</sup> and R. D’Arcy<sup>1,\*\*</sup>

<sup>1</sup>*Deutsches Elektronen-Synchrotron DESY, Germany*

<sup>2</sup>*Paul Scherrer Institut, Switzerland*

<sup>3</sup>*Department of Physics Universität Hamburg, Germany*

(Dated: March 13, 2025)

Detailed knowledge of particle-beam properties is of great importance to understand and push the performance of existing and next-generation particle accelerators. We recently proposed a new phase-space tomography method to reconstruct the five-dimensional (5D) phase space, i.e., the charge density distribution in all three spatial directions and the two transverse momenta. Here, we present the first experimental demonstration of the method at the FLASHForward facility at DESY. This includes the reconstruction of the 5D phase-space distribution of a GeV-class electron bunch, the use of this measured phase space to create a particle distribution for simulations, and the extraction of the transverse 4D slice emittance.

Particle accelerators are highly complex and multivariate machines that are required to produce beams with percent- to permille-level stability at highly specialized working points with limited diagnostics. The generation of these beams is especially difficult for applications that require excellent phase-space quality such as advanced ultra-high-gradient accelerators [1–10] or free-electron lasers [11–18], and their complex operation modes (e.g. two-color lasing [19, 20]).

To characterize these electron beams, methods focusing on the reconstruction of statistical beam parameters or 2-dimensional (2D) projections of the full phase space [21–26] are routinely used. For higher-dimensional structures, especially when correlations between the transverse and longitudinal phase spaces are present, the above mentioned techniques are insufficient. Tomographic methods have been successfully applied to these cases, e.g., for measuring the time-resolved transverse phase-space distribution [27], the full 4D transverse phase space [28–31], as well as the full 3D spatial distribution [32–35].

The development of the polarizable X-band transverse deflection structure (Polarix TDS) [35–37] by a collaboration of scientists from CERN, PSI, and DESY enables the extension of these existing diagnostics abilities [32, 35, 38] to include streaking of the bunch in any transverse direction. Based on this capability, we recently proposed a new method that extends the existing tomographic methods by an extra dimension and reconstructs the full 5D phase-space density of bunches [39], i.e., the transverse positions  $(x, y)$  and divergences

$(x', y')$  as well as the time coordinate  $t$ . This technique combines a quadrupole-based 4D transverse tomography [28] in normalized phase space with the streaking of the bunch along various directions by the Polarix TDS. Simulation studies of the 5D tomography method have shown the successful reconstruction of the 5D phase space of complex beam distributions [39].

Other methods have been studied to obtain higher dimensional information. For sub-relativistic beams, a combination of horizontal and vertical slit masks can be used and has been benchmarked with a 2.5 MeV H<sup>-</sup> beam for 5D [40], and 6D [41] reconstructions. Furthermore, machine learning based approaches are gaining popularity, which focus on predicting phase-space projections [42–45] up to the full 6D particle distribution [46]. While these methods show promising results, the obtained distribution is only a prediction ensured to match very limited beam measurements.

In this letter, we focus on the use of tomographic methods that are based on direct measurements of all relevant phase-space projections. We present the first 5D tomographic reconstruction of an electron bunch as well as self-consistent checks to validate the results. We show that the method resolves previously hidden correlations between all the transverse planes and time coordinate and in addition allows the 4D slice emittance to be extracted. Furthermore, by propagating the reconstructed 5D distribution along the beamline, new possibilities open up for performing highly accurate simulation studies to understand and optimize the accelerator performance or to benchmark the results of simulation codes.

The measurement campaign was performed at the FLASHForward facility [47] which is dedicated to beam-driven plasma-acceleration experiments. It uses the high-quality and stable electron bunches provided by the FLASH linear accelerator [11, 48, 49]. A sketch of the relevant beamline section is shown in Fig. 1. To record the beam images, a screen station downstream of the Polarix TDS was used with Scheimpflug optics,

\* [sonja.jaster-merz@desy.de](mailto:sonja.jaster-merz@desy.de)

† Present address: 1

‡ Present address: 2

§ Present address: 3

¶ Present address: Lawrence Berkeley National Laboratory, Berkeley, California 94720, USA

\*\* Present address: 5

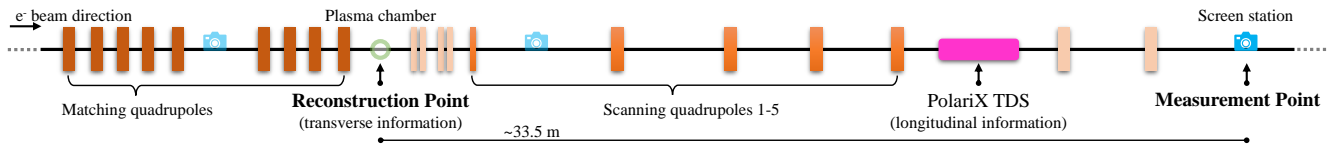


FIG. 1. The FLASHForward beamline section used for the 5D tomography measurement. The transverse phase space is reconstructed at the location labeled as the reconstruction point. The reconstruction of the time information is obtained at the PolariX TDS. The screen images for the tomography were recorded at the measurement point. Beamline elements that were not used for the measurement are displayed in a fainter color.

80 a Cerium-doped Gadolinium Aluminum Gallium Garnet  
 81 (GAGG:Ce) scintillating screen, and a nominal resolution  
 82 of  $10\ \mu\text{m}$  [50]. Nine quadrupoles were operated to set the  
 83 beam optics [51] to  $\beta_x = \beta_y = 10\ \text{m}$  and  $\alpha_x = \alpha_y = 0$  at  
 84 the reconstruction point. The 5D tomography method  
 85 [39] simultaneously controls the horizontal and vertical  
 86 phase advances between the reconstruction point and  
 87 measurement point. These phase advances were varied  
 88 using five quadrupoles covering a range of  $180^\circ$  in ten  
 89 steps in both transverse planes. The required quadrupole  
 90 strengths were determined in simulations. For each phase  
 91 advance combination, the beam was streaked using the  
 92 PolariX TDS at ten transverse angles covering approxi-  
 93 mately  $180^\circ$ . This resulted in a total of 1000 planned scan  
 94 steps. All quadrupoles between the TDS and measure-  
 95 ment screen were switched off as identical beam optics  
 96 in all transverse directions between these points are re-  
 97 quired for the tomographic reconstruction of the charge  
 98 density [33].

99 The shear parameter, relating the measured transverse  
 100 coordinate along the streaking direction at the measure-  
 101 ment point to the longitudinal position within the bunch  
 102 at the TDS location, was measured for all streaking an-  
 103 gles by means of a radio-frequency (RF) phase scan. The  
 104 PolariX amplitude was set to the maximum of the avail-  
 105 able RF power at an average value of  $4.5\ \text{MW} \pm 0.3\ \text{MW}$   
 106 resulting in an average shear parameter of  $18.7 \pm 2.5$ .  
 107 The beta function at the measurement point was kept ap-  
 108 proximately at  $\beta_x = \beta_y = 10\ \text{m}$  to obtain a near-constant  
 109 longitudinal resolution in the tens-of-fs range while main-  
 110 taining an achievable optics setup for the beamline.

111 For the 5D phase-space-tomography measurement, the  
 112 quadrupoles were cycled between scan points whenever  
 113 their ramping direction was changed to prevent hystere-  
 114 sis effects. For each scan point, ten screen images with  
 115 beam as well as ten background images were recorded.  
 116 In addition, screen images of the unstreaked beam were  
 117 collected. During the experiment, 960 out of 1000 scan  
 118 points were recorded successfully in 28 h. Charge and  
 119 compression feedbacks were enabled to obtain a stable  
 120 beam with RMS variations below 1% for the charge and  
 121 below 8% for the bunch length over the entire measure-  
 122 ment. The measurement was conducted at a beam en-  
 123 ergy of  $1.09\ \text{GeV} \pm 0.01\ \text{GeV}$  and with an average beam  
 124 charge of  $297\ \text{pC} \pm 2\ \text{pC}$ .

125 The 5D tomographic reconstruction procedure is de-  
 126 scribed in detail in reference [39]. A Python scikit-image

127 implementation of the SART (Simultaneous Algebraic  
 128 Reconstruction Technique) algorithm [52, 53] was used  
 129 with two iterations. In a first step, the 3D charge-density  
 130 distribution was reconstructed [32] at the measurement  
 131 location for each phase-advance combination. This dis-  
 132 tribution was then converted into normalized coordinates  
 133 using the Courant-Snyder parameters [51] at this location  
 134 obtained from simulations. For each time slice of the  
 135 bunch, the transverse distributions of all phase advance  
 136 settings were combined and the 4D phase space was re-  
 137 constructed using a method similar to the one presented  
 138 in [28]. Finally, by joining all time slices the 5D distri-  
 139 bution  $(x_N, x'_N, y_N, y'_N, t)$  was obtained. The time infor-  
 140 mation was reconstructed at the location of the PolariX  
 141 TDS using 72 slices of 20 fs duration, with the duration  
 142 approximately corresponding to the average longitudinal  
 143 resolution of  $19\ \text{fs} \pm 5\ \text{fs}$ . The transverse information was  
 144 reconstructed upstream of the five scanning quadrupoles  
 145 (see Fig. 1) with 301 bins in each transverse direction in  
 146 a range of  $\pm 5 \times 10^{-4}\ \text{m}/\sqrt{\text{m}}$  corresponding to an approx-  
 147 imate bin size of the assumed  $10\ \mu\text{m}$  screen resolution.  
 148 A constant beam charge was assumed in all tomographic  
 149 reconstructions.

150 The projection of the reconstructed 5D phase space  
 151 onto the ten 2D planes is shown in Fig. 2. Non-linear  
 152 correlations between all transverse planes and the time  
 153 coordinate are visible. The projected normalized trans-  
 154 verse phase spaces deviate from the matched circular case  
 155 and exhibit non-Gaussian structures which are visible es-  
 156 pecially in the  $(x'_N, y'_N)$  and  $(y_N, y'_N)$  planes. These fea-  
 157 tures mainly stem from varying centroid and momentum  
 158 offsets along the bunch. Such correlations can appear  
 159 in linear accelerators and can be caused by collective ef-  
 160 fects, such as space charge and coherent synchrotron ra-  
 161 diation (CSR) occurring, e.g., during the compression of  
 162 the bunch [54, 55]. In particular, the correlations in the  
 163  $(x_N, t)$  plane are expected to originate from CSR effects  
 164 induced in the two horizontal bunch compressor chicane  
 165 located upstream in the FLASH linac, as qualitatively  
 166 similar features have also been observed in previous sim-  
 167 ulation studies [32, 34]. The correlations in the  $(y'_N, t)$   
 168 phase space cannot be explained by these CSR effects.  
 169 We believe that these correlations are caused by the re-  
 170 maining vertical dispersion in the beamline which, in  
 171 combination with the induced energy chirp during bunch  
 172 compression, would lead to correlations between the ver-  
 173 tical planes and the time coordinate. An optimization of

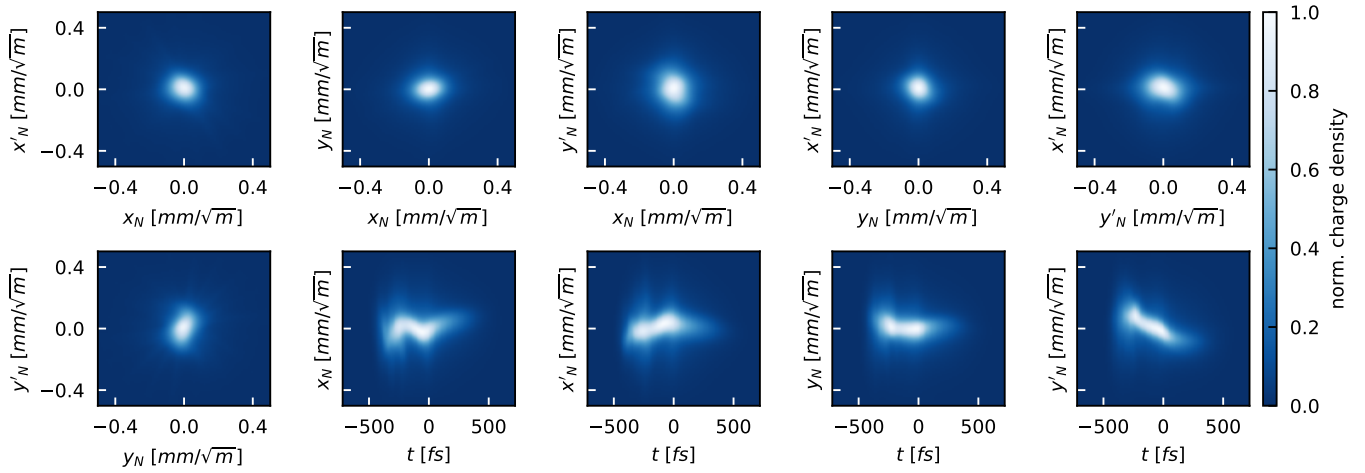


FIG. 2. 2D projections of the reconstructed 5D phase-space distribution normalized to their maximum value. The transverse projections are shown in normalized phase space. The head of the bunch is towards negative time values.

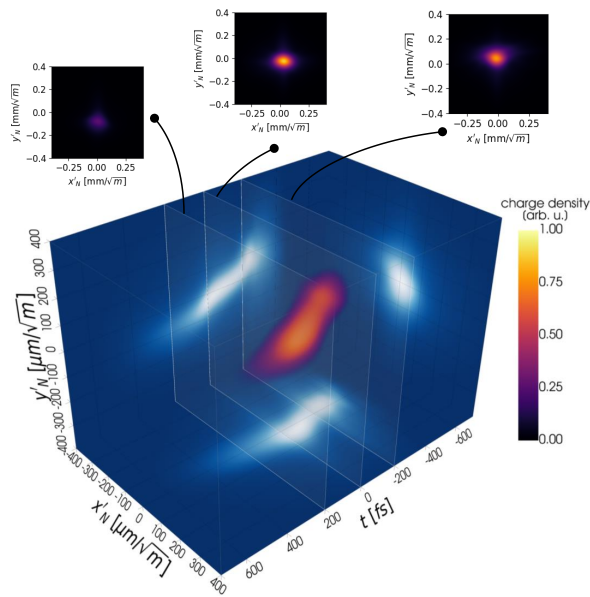


FIG. 3. Rendering of the reconstructed 5D phase space distribution projected onto the  $(x'_N, y'_N, t)$  phase space. The projection is normalized to the maximum value of the charge density. In addition, the 2D projections are displayed in blue color and exemplarily three transverse slices are included.

174 the observed correlations was beyond the scope of this  
 175 proof-of-principle demonstration but is now possible due  
 176 to the ability of the 5D tomography method to unveil  
 177 these effects.

178 In addition to the 2D projections, the projection onto  
 179 the 3D  $(x'_N, y'_N, t)$  phase space is shown in Fig. 3, high-  
 180 lighting three transverse slices along the bunch. The  
 181 aforementioned features and non-linear correlations, as  
 182 well as momentum offsets, are also visible here.

183 Furthermore, the reconstruction can be used to cre-  
 184 ate a particle distribution with a significant number of

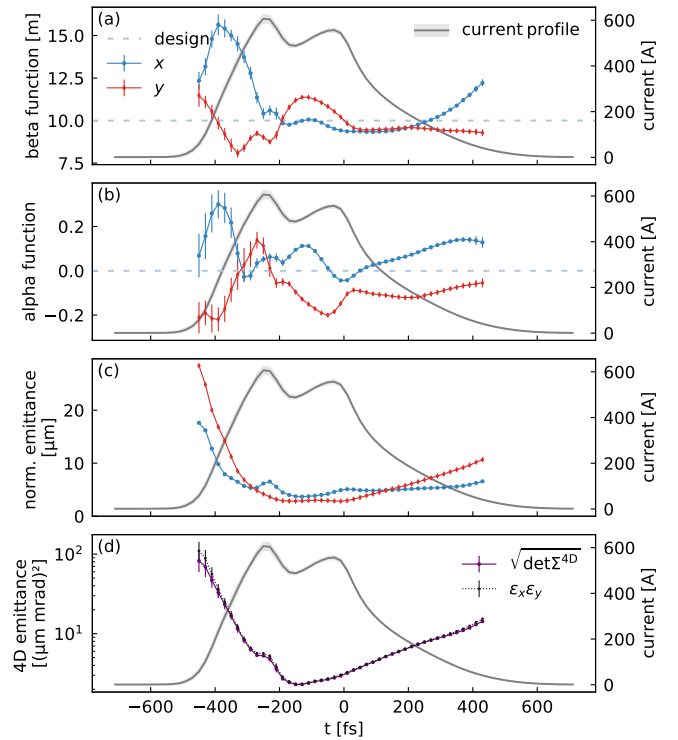


FIG. 4. Reconstructed current profile, (a) beta functions, (b) alpha functions, and (c) sliced normalized transverse emittances for both transverse planes obtained from the 5D charge density. (d) The sliced 4D emittance is compared to the value obtained when multiplying the two transverse emittances. Only slices that contain at least 10 000 particles (0.2% of the total charge) are analyzed and the errorbars are obtained from 100 reconstructions where the shear parameter of each streaking angle is randomly sampled from a Gaussian distribution with a one sigma measurement uncertainty.

macro particles, in the presented case five million. The distribution is generated slice-wise by randomly creating particles in accordance with the probability distribution of the reconstructed phase space. Only probability values larger than 5% of the maximum value of each slice are appropriately populated. This threshold has been found to be a good balance between removing noise introduced by the tomographic reconstruction, typically occurring far off-axis and arising due to the finite amount of projection angles [35], and preserving the features of the reconstructed distribution. The obtained distribution is used to calculate the beam covariance matrix  $\Sigma^{4D}$  for all slices containing at least 10 000 particles and extract the slice beam parameters shown in Fig. 4 like the transverse Courant-Snyder parameters, normalized emittances  $\epsilon_x^n, \epsilon_y^n$  and the current profile. Variations of these parameters along the bunch are visible as well as a mismatch to the design values of  $\beta = 10$  m and  $\alpha = 0$ . In addition, the sliced 4D emittance  $\epsilon^{4D} = \sqrt{\det \Sigma^{4D}}$  is extracted. It is a measure of the minimum transverse emittances that can be reached in the case that all correlations between the planes are eliminated [56]. As the lasing performance of FELs and the luminosity of colliders depend on the transverse emittances [57, 58], having the ability to now measure and in the future correct for correlations is highly beneficial. The measured sliced 4D emittance is shown in Fig. 4 (d) and compared to a multiplication of the two transverse emittances  $\epsilon_{\text{approx}}^{4D} = \epsilon_x \epsilon_y$ , which are accessible with conventional PolariX TDS measurements. The average relative discrepancy is 5% with a minimum of 1% at around  $-170$  fs. The measurement therefore indicates that only minor correlations between the transverse planes are present which are minimal at the core part of the bunch.

The tomographic reconstruction is validated using two approaches. First, the beam parameters obtained from the tomographic reconstruction are compared to lower dimensional complementary measurements listed in Table I. To obtain the normalized transverse RMS emittances and Courant-Snyder parameters, a multi-quadrupole scan analysis is performed using the unstreaked beam images. The uncertainties are obtained from statistical fluctuation from ten different datasets recorded throughout the 5D tomography measurement. The uncertainty on the tomographic reconstruction is estimated by performing 100 reconstructions using the Python library Optimas [59] where the shear parameter of each streaking angle is randomly sampled from a Gaussian distribution and a one sigma measurement uncertainty is applied. In addition, errors on the reconstruction due to an energy uncertainty (a 1% energy error results in a 5% emittance error), an energy spread within the distribution (a projected RMS energy spread of 1% consisting of a linear energy chirp and an uncorrelated RMS energy spread of 0.1% result in a 2% emittance error), and due to the finite number of projection angles (ten angles per plane result in an overestimation of the emittance by up to 13%) are expected. While these

measurement errors are expected to apply equally to both transverse planes, we suspect that the larger discrepancy in the vertical emittance can be explained by an incomplete dataset of the last vertical phase advance scan (and hence a reduced number of recorded projections compared to the horizontal plane) resulting in an increased measurement uncertainty in this plane. The discrepancies in the alpha functions cannot be explained by the expected measurement uncertainties of the two methods. The beta functions and horizontal emittance agree well between the two methods within the estimated uncertainties. The bunch duration is determined using the screen images of the streaked beam at both zero crossings. Following [60, 61], linear correlations within the bunch are taken into account resulting in an RMS bunch duration of  $194 \text{ fs} \pm 16 \text{ fs}$  which is in excellent agreement with the result of  $199^{+8}_{-7} \text{ fs}$  obtained from the tomography.

Second, the obtained particle distribution from the reconstructed 5D phase space is tracked from the reconstruction point to the measurement point for all beam-line settings that were used in the measurement. The obtained simulated screen images of the distribution are then compared to the measured ones. This comparison is done in the  $(v, t)$  coordinates, where  $v$  is the transverse plane perpendicular to the streaking direction and  $t$  is the time axis obtained by scaling the streaking plane with the shear parameter. As a measure of deviation between the reconstructed and measured projections, the deviations between the centroid position of each time slice normalized to the RMS spread of the measured distribution are determined, and the average weighted by the slice charge is calculated. Only slices that contain more than 0.5% of the total charge are taken into account. The average relative discrepancy for all recorded projections is  $32\% \pm 15\%$ . A visual comparison of the measured and tracked screen images shows that for most projections a qualitatively accurate reconstruction of the beam shape is obtained, as can be seen in a subset of the data shown in Fig. 5. The main discrepancy between the measured and tracked projections is expected to stem from a blurring and loss of small beam features, which are especially sensitive to uncertainties in the shear parameter, as well as small changes in the distribution over the measurement time.

Overall, the two validations indicate a reasonable agreement of the reconstructed 5D distribution with lower-dimensional complementary measurements and thereby support the experimental usability of the 5D tomography method.

In this work we presented the first tomographic reconstruction of the 5D phase space of an electron beam and the validation of the result against lower dimensional projections. The 2D projections of the reconstructed phase space show correlations between the transverse and longitudinal planes that were not detectable with previous diagnostic methods. Furthermore, the tomographic reconstruction facilitated the first sliced 4D emittance measurement at a free-electron laser. While the recon-

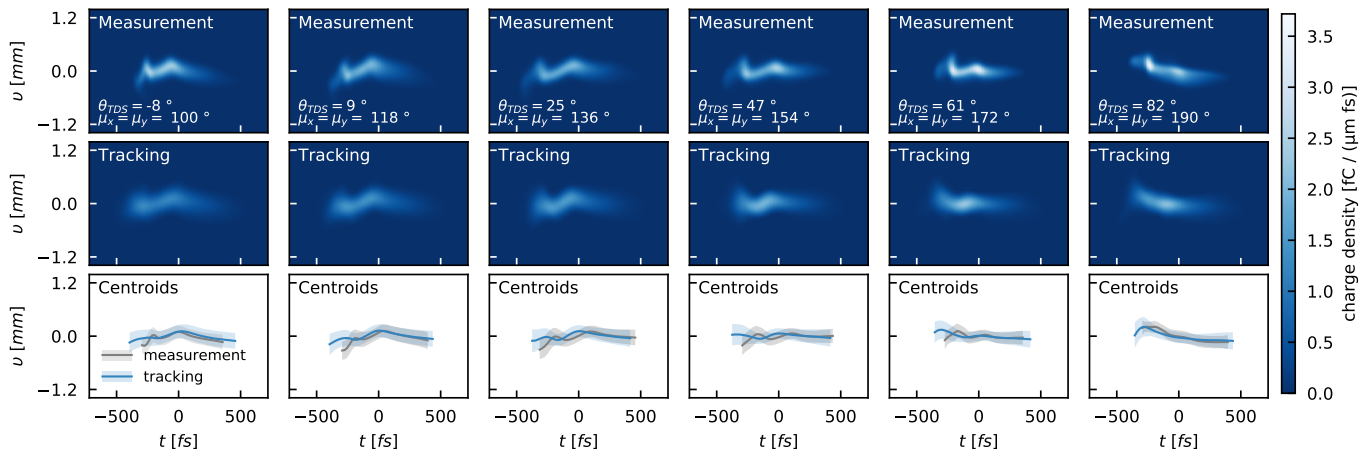


FIG. 5. Comparison of the measured screen images (top) to the tracked distribution (middle) for various phase advances  $\mu_x, \mu_y$ . The screen images are rotated by the streaking angle  $\theta_{TDS}$  and the projection in streaking direction is converted to the time axis. The coordinate  $v$  denotes the transverse plane of the bunch perpendicular to the streaking plane. The bottom row shows the centroid positions and RMS spread for each time slice containing more than 0.5% of the total charge.

TABLE I. Reconstructed Beam Parameters

Param.	Units	Tomography	Quad. scan
$\epsilon_x^n$	$\mu\text{m}$	$6.63 \pm 0.10$	$6.22 \pm 0.68$
$\epsilon_y^n$	$\mu\text{m}$	$8.25 \pm 0.20$	$6.69 \pm 0.62$
$\alpha_x$	-	$0.09 \pm 0.00$	$0.37 \pm 0.08$
$\alpha_y$	-	$-0.28 \pm 0.01$	$0.05 \pm 0.14$
$\beta_x$	m	$10.75 \pm 0.04$	$11.74 \pm 1.50$
$\beta_y$	m	$7.44 \pm 0.05$	$7.04 \pm 0.61$
$\sigma_t$	fs	$199_{-7}^{+8}$	$194 \pm 16^a$

<sup>a</sup> Obtained from streaked screen images at both zero crossings.

301 structured bunch was not optimized for FEL or plasma  
 302 operation, both applications can benefit from the pre-  
 303 sented measurement method as undesired correlations  
 304 that either degrade the transverse emittances (and hence  
 305 the lasing performance of FELs) or drive instabilities in  
 306 beam-driven plasma accelerators [2, 62, 63] can be iden-  
 307 tified and minimized. Furthermore, conversion of the re-  
 308 constructed phase space into a particle distribution en-  
 309 ables highly realistic simulations of the beamline with  
 310 the potential to better understand and improve its per-  
 311 formance. A future combination of such a 5D tomogra-  
 312 phy with an additional longitudinal phase space measure-  
 313 ment would provide a quasi-complete characterization of  
 314 electron beams. These results can additionally be used  
 315 to benchmark other diagnostic methods, e.g., based on  
 316 machine learning [46] which use only minimal beam pro-  
 317 jections to infer the particle distribution.

318 To increase the viability of the measurement, a reduc-  
 319 tion of the measurement time is strongly desired. Dur-  
 320 ing the measurement campaign we could already show  
 321 that an optimized operation of the PolariX RF ampli-  
 322 tude while changing the streaking angle reduces the mea-  
 323 surement time by up to 30%. The remaining dominant  
 324 factor was the cycling of the quadrupoles. If the mea-

325 surement is modified in such a way that no cycling is  
 326 needed, the measurement time can be reduced substan-  
 327 tially. Proof-of-principle tests in this direction at the  
 328 ARES accelerator [64] have in fact been shown to reduce  
 329 the measurement time by up to 80% [31]. Finally, the  
 330 use of machine-learning-assisted reconstruction methods  
 331 could be explored to reduce the number of required pro-  
 332 jections [46, 65].

333 We would like to thank S. Schreiber and the scien-  
 334 tific committee at FLASH for supporting this study and  
 335 providing us with this beamtime, M. Vogt for the sup-  
 336 port on the PolariX structures, as well as the FLASH  
 337 operators for their support during the beamtime. We  
 338 thank the technical groups for their support, especially  
 339 R. Jonas for helpful advice on the operation of the Po-  
 340 lariX phase shifter. Furthermore, we thank A. Wolski  
 341 for helpful discussions on optimizing the beamline for the  
 342 tomographic measurement, A. Ferran Pousa for helpful  
 343 discussions on the data analysis and the support on the  
 344 optimas library, and B. Beutner for the helpful discus-  
 345 sions on the results. This research was supported in part  
 346 through the Maxwell computational resources operated  
 347 at Deutsches Elektronen-Synchrotron DESY, Hamburg,  
 348 Germany. We acknowledge support from DESY (Ham-  
 349 burg, Germany), a member of the Helmholtz Association  
 350 HGF.

351 SJM, RA, RB, FB, WH, MS, and TV conceptualized  
 352 the work and proposed the experimental demonstration.  
 353 SJM, FB, PGC, and RD planned the experiment. SJM,  
 354 PGC, FM, and SW conducted preparatory work for the  
 355 experiment. SJM, JB, JBS, FB, PC, RD, HD, PGC, AK,  
 356 MK, WK, FM, BS, TV, and SW conducted the experi-  
 357 ment. SJM performed the data analysis and wrote the  
 358 manuscript. JB, FB, PC, RD, HD, MK, WK, FM, TV,  
 359 and SW contributed to the manuscript. Everybody read  
 360 the manuscript and contributed to discussions of the re-  
 361 sults.

- [1] P. Chen *et al.*, Acceleration of electrons by the interaction of a bunched electron beam with a plasma, *Phys. Rev. Lett.* **54**, 693 (1985).
- [2] D. H. Whittum *et al.*, Electron-hose instability in the ion-focused regime, *Phys. Rev. Lett.* **67**, 991 (1991).
- [3] M. Galletti *et al.*, Stable operation of a free-electron laser driven by a plasma accelerator, *Phys. Rev. Lett.* **129**, 234801 (2022).
- [4] C. Joshi *et al.*, Plasma wakefield acceleration experiments at FACET II, *Plasma Physics and Controlled Fusion* **60**, 034001 (2018).
- [5] E. o. Adli, Acceleration of electrons in the plasma wakefield of a proton bunch, *Nature* **561**, 363 (2018).
- [6] I. Blumenfeld *et al.*, Energy doubling of 42 GeV electrons in a metre-scale plasma wakefield accelerator, *Nature* **445**, 741 (2007).
- [7] M. Litos *et al.*, High-efficiency acceleration of an electron beam in a plasma wakefield accelerator, *Nature* **515**, 92 (2014).
- [8] M. Ferrario *et al.*, SPARCLAB present and future, *Nuclear Instruments and Methods in Physics Research Section B: Beam Interactions with Materials and Atoms* **309**, 183 (2013).
- [9] R. Pompili *et al.*, Free-electron lasing with compact beam-driven plasma wakefield accelerator, *Nature* **605**, 659 (2022).
- [10] B. Hidding *et al.*, Progress in hybrid plasma wakefield acceleration, *Photonics* **10**, 10.3390/photonics10020099 (2023).
- [11] J. Rossbach *et al.*, 10 years of pioneering X-ray science at the Free-Electron Laser FLASH at DESY, *Phys. Rep.* **808**, 1 (2019).
- [12] R. Abela *et al.*, *XFEL: The European X-Ray Free-Electron Laser - Technical Design Report* (DESY, Hamburg, 2006) pp. 1–646.
- [13] P. Emma *et al.*, First lasing and operation of an ångström-wavelength free-electron laser, *Nature Photonics* **4**, 641 (2010).
- [14] T. Ishikawa *et al.*, A compact x-ray free-electron laser emitting in the sub-ångström region, *Nature Photonics* **6**, 540 (2012).
- [15] L. Giannessi *et al.*, Status and Perspectives of the FERMI FEL Facility (2019), in *Proc. FEL'19*, Free Electron Laser Conference No. 39 (JACoW Publishing, Geneva, Switzerland, 2019) pp. 742–745.
- [16] H.-S. Kang *et al.*, Hard x-ray free-electron laser with femtosecond-scale timing jitter, *Nature Photonics* **11**, 708 (2017).
- [17] E. Prat *et al.*, A compact and cost-effective hard x-ray free-electron laser driven by a high-brightness and low-energy electron beam, *Nature Photonics* **14**, 748 (2020).
- [18] B. Liu *et al.*, The SXFEL upgrade: from test facility to user facility, *Applied Sciences* **12**, 176 (2021).
- [19] E. Ferrari *et al.*, Widely tunable two-colour seeded free-electron laser source for resonant-pump resonant-probe magnetic scattering, *Nature Communications* **7**, 10.1038/ncomms10343 (2016).
- [20] E. Prat *et al.*, Widely tunable two-color x-ray free-electron laser pulses, *Phys. Rev. Res.* **4**, L022025 (2022).
- [21] C. McKee *et al.*, Phase space tomography of relativistic electron beams, *Nucl. Instrum. Methods Phys. Res., Sect. A* **358**, 264 (1995).
- [22] D. Stratakis *et al.*, Tomography as a diagnostic tool for phase space mapping of intense particle beams, *Phys. Rev. Accel. Beams* **9**, 112801 (2006).
- [23] V. Yakimenko *et al.*, Electron beam phase-space measurement using a high-precision tomography technique, *Phys. Rev. Accel. Beams* **6**, 122801 (2003).
- [24] B. Hermann *et al.*, Electron beam transverse phase space tomography using nanofabricated wire scanners with submicrometer resolution, *Phys. Rev. Accel. Beams* **24**, 022802 (2021).
- [25] D. Dowell *et al.*, Longitudinal emittance measurements at the SLAC gun test facility, *Nucl. Instrum. Methods Phys. Res., Sect. A* **507**, 331 (2003), proceedings of the 24th International Free Electron Laser Conference and the 9th Users Workshop.
- [26] D. Malyutin *et al.*, Longitudinal phase space tomography using a booster cavity at PITZ, *Nucl. Instrum. Methods Phys. Res., Sect. A* **871**, 105 (2017).
- [27] M. Röhrs, C. Gerth, H. Schlarb, B. Schmidt, and P. Schmäser, Time-resolved electron beam phase space tomography at a soft x-ray free-electron laser, *Phys. Rev. Accel. Beams* **12**, 050704 (2009).
- [28] K. Hock *et al.*, Tomographic reconstruction of the full 4D transverse phase space, *Nucl. Instrum. Methods Phys. Res., Sect. A* **726**, 8 (2013).
- [29] A. Wolski *et al.*, Transverse phase space characterization in an accelerator test facility, *Phys. Rev. Accel. Beams* **23**, 032804 (2020).
- [30] V. Guo, P. Denham, P. Musumeci, A. Ody, and Y. Park, 4D Beam Tomography at the UCLA Pegasus Laboratory, in *Proc. IBIC'21*, International Beam Instrumentation Conference (JACoW Publishing, Geneva, Switzerland, 2021) pp. 227–231.
- [31] S. Jaster-Merz *et al.*, Characterization of the full transverse phase space of electron bunches at ARES, in *Proc. IPAC'21*, 12th Int. Particle Accelerator Conf. (IPAC'21), Campinas, Brazil (2021).
- [32] D. Marx *et al.*, Reconstruction of the 3D charge distribution of an electron bunch using a novel variable-polarization transverse deflecting structure (TDS), *J. Phys. Conf. Ser.* **874**, 012077 (2017).
- [33] D. Marx *et al.*, Simulation studies for characterizing ultrashort bunches using novel polarizable X-band transverse deflection structures, *Sci. Rep.* **9**, 19912 (2019).
- [34] D. Marx, *Characterization of Ultrashort Electron Bunches at the SINBAD-ARES Linac*, *Dissertation*, Universität Hamburg, Hamburg, Germany (2019).
- [35] B. Marchetti *et al.*, Experimental demonstration of novel beam characterization using a polarizable X-band transverse deflection structure, *Sci. Rep.* **11**, 3560 (2021).
- [36] P. Craievich *et al.*, Novel X-band transverse deflection structure with variable polarization, *Phys. Rev. Accel. Beams* **23**, 112001 (2020).
- [37] A. Grudiev, design of compact high power rf components at x-band, *CLIC note* (2016).
- [38] P. González Caminal *et al.*, Beam-based commissioning of a novel x-band transverse deflection structure with variable polarization, *Phys. Rev. Accel. Beams* **27**, 032801 (2024).
- [39] S. Jaster-Merz, R. W. Assmann, R. Brinkmann,

- 484 F. Burkart, W. Hillert, M. Stanitzki, and T. Vinatier, 5D tomographic phase-space reconstruction of particle  
485 bunches, *Phys. Rev. Accel. Beams* **27**, 072801 (2024).  
486
- 487 [40] A. Hoover, K. Ruisard, A. Aleksandrov, A. Zhukov,  
488 and S. Cousineau, Analysis of a hadron beam in five-  
489 dimensional phase space, *Phys. Rev. Accel. Beams* **26**,  
490 064202 (2023).
- 491 [41] B. Cathey, S. Cousineau, A. Aleksandrov, and A. Zhukov,  
492 First six dimensional phase space measurement of an ac-  
493 celerator beam, *Phys. Rev. Lett.* **121**, 064804 (2018).
- 494 [42] H. Yutao, L. Renkai, and W. Weishi, *Measurement of  
495 transverse phase space based on machine learning* (2023).
- 496 [43] A. Scheinker, A. Edelen, D. Bohler, C. Emma, and  
497 A. Lutman, Demonstration of model-independent control  
498 of the longitudinal phase space of electron beams in the  
499 linac-coherent light source with femtosecond resolution,  
500 *Phys. Rev. Lett.* **121**, 044801 (2018).
- 501 [44] A. Scheinker, F. W. Cropp V, and D. Filippetto, 6D  
502 Phase Space Diagnostics Based on Adaptively Tuned  
503 Physics-Informed Generative Convolutional Neural Net-  
504 works, in *Proc. IPAC'22*, Proceedings of the 13th Inter-  
505 national Particle Accelerator Conference, Bangkok,  
506 Thailand (2022) pp. 776–779.
- 507 [45] A. Scheinker, F. Cropp, and D. Filippetto, Adaptive  
508 autoencoder latent space tuning for more robust ma-  
509 chine learning beyond the training set for six-dimensional  
510 phase space diagnostics of a time-varying ultrafast  
511 electron-diffraction compact accelerator, *Phys. Rev. E*  
512 **107**, 045302 (2023).
- 513 [46] R. Roussel, J. P. Gonzalez-Aguilera, E. Wisniewski,  
514 A. Ody, W. Liu, J. Power, Y.-K. Kim, and A. Ede-  
515 len, Efficient six-dimensional phase space reconstructions  
516 from experimental measurements using generative ma-  
517 chine learning, *Phys. Rev. Accel. Beams* **27**, 094601  
518 (2024).
- 519 [47] R. D'Arcy *et al.*, Flashforward: plasma wakefield ac-  
520 celerator science for high-average-power applications, *Phil.  
521 Trans. R. Soc. A* **377**, 20180392 (2019).
- 522 [48] S. Schreiber *et al.*, The free-electron laser FLASH, *High  
523 Power Laser Sci. Eng.* **3**, e20 (2015).
- 524 [49] W. Ackermann *et al.*, Operation of a free-electron laser  
525 from the extreme ultraviolet to the water window, *Nat.  
526 Photonics* **1**, 336 (2007).
- 527 [50] C. Wiebers *et al.*, Scintillating Screen Monitors for Trans-  
528 verse Electron Beam Profile Diagnostics at the European  
529 XFEL, in *Proc. IBIC'13* (JACoW Publishing, Geneva,  
530 Switzerland, 2013) pp. 807–810.
- 531 [51] E. Courant and H. Snyder, Theory of the alternating-  
532 gradient synchrotron, *Annals of Physics* **3**, 1 (1958).
- 533 [52] A. Andersen and A. Kak, Simultaneous Algebraic Recon-  
534 struction Technique (SART): A superior implementation  
535 of the ART algorithm, *Ultrason. Imaging* **6**, 81 (1984).
- 536 [53] S. Van der Walt *et al.*, scikit-image: image processing in  
537 Python, *PeerJ* **2**, e453 (2014).
- 538 [54] Y. S. Derbenev, J. Rossbach, E. L. Saldin, and V. D.  
539 Shiltsev, *Microbunch radiative tail - head interaction*,  
540 Tech. Rep. TESLA-FEL 1995-05 (DESY, 1995).
- 541 [55] M. Dohlus *et al.*, Bunch Compression for Linac-Based  
542 FEL's. Electron Bunch Length Compression, *ICFA Beam  
543 Dynamics Newsletter* **38** (2006).
- 544 [56] L. Z. Rivkin, *Damping ring for the SLAC linear collider*,  
545 *Ph.D. thesis*, California Institute of Technology (1986).
- 546 [57] E. Prat and M. Aiba, Four-dimensional transverse beam  
547 matrix measurement using the multiple-quadrupole scan  
548 technique, *Phys. Rev. ST Accel. Beams* **17**, 052801  
549 (2014).
- 550 [58] M. Aicheler, P. Burrows, M. Draper, T. Garvey, P. Le-  
551 brun, K. Peach, N. Phinney, H. Schmickler, D. Schulte,  
552 and N. Toge, *A Multi-TeV Linear Collider Based on  
553 CLIC Technology: CLIC Conceptual Design Report*,  
554 CERN Yellow Reports: Monographs (CERN, Geneva,  
555 2012).
- 556 [59] A. Ferran Pousa, S. Jalas, M. Kirchen, A. Martinez de la  
557 Ossa, M. Thévenet, S. Hudson, J. Larson, A. Huebl, J.-L.  
558 Vay, and R. Lehe, Bayesian optimization of laser-plasma  
559 accelerators assisted by reduced physical models, *Phys.  
560 Rev. Accel. Beams* **26**, 084601 (2023).
- 561 [60] P. Emma *et al.*, Bunch Length Measurements Using a  
562 Transverse RF Deflecting Structure in the SLAC Linac,  
563 in *Proc. EPAC'02* (JACoW Publishing, Geneva, Switzer-  
564 land, 2002) pp. 1882–1884.
- 565 [61] C. Behrens *et al.*, Few-femtosecond time-resolved mea-  
566 surements of x-ray free-electron lasers, *Nature Commu-  
567 nications* **5**, 3762 (2014).
- 568 [62] C. Huang, W. Lu, M. Zhou, C. E. Clayton, C. Joshi,  
569 W. B. Mori, P. Muggli, S. Deng, E. Oz, T. Katsouleas,  
570 M. J. Hogan, I. Blumenfeld, F. J. Decker, R. Ischebeck,  
571 R. H. Iverson, N. A. Kirby, and D. Walz, Hosing insta-  
572 bility in the blow-out regime for plasma-wakefield ac-  
573 celeration, *Phys. Rev. Lett.* **99**, 255001 (2007).
- 574 [63] T. J. Mehrling, R. A. Fonseca, A. Martinez de la  
575 Ossa, and J. Vieira, Mitigation of the hose instability  
576 in plasma-wakefield accelerators, *Phys. Rev. Lett.* **118**,  
577 174801 (2017).
- 578 [64] F. Burkart *et al.*, The ARES Linac at DESY, in *Proc.  
579 LINAC'22*, International Linear Accelerator Conference  
580 No. 31 (JACoW Publishing, Geneva, Switzerland, 2022)  
581 pp. 691–694.
- 582 [65] A. Hoover and J. C. Wong, High-dimensional maximum-  
583 entropy phase space tomography using normalizing flows,  
584 *Phys. Rev. Res.* **6**, 033163 (2024).